PAPER

View Article Online
View Journal | View Issue

Structural predictions of three medium-sized thiolate-protected gold nanoclusters $Au_{44}(SR)_{30}$, $Au_{56}(SR)_{32}$, and $Au_{60}(SR)_{34}$†

Wenhua Han,‡[a] Gang Wang,‡[a] Pengye Liu,[b] Wenliang Li*[a] and Wen Wu Xu [iD] *[b]

The knowledge of structural evolution among thiolate-protected gold nanoclusters is not only helpful for understanding their structure–property relationship but also provides scientific evidence to rule-guided structure predictions of gold nanoclusters. In this paper, three new atomic structures of medium-sized thiolate-protected gold nanoclusters, *i.e.* $Au_{44}(SR)_{30}$, $Au_{56}(SR)_{32}$, and $Au_{60}(SR)_{34}$, are predicted based on the grand unified model and ring model. Two structural evolution rules, *i.e.*, $Au_{44}(SR)_{28} + [Au_{12}(SR)_4] \rightarrow Au_{56}(SR)_{32} + [Au_{12}(SR)_4] \rightarrow Au_{68}(SR)_{36}$ and $Au_{44}(SR)_{30} + [Au_8(SR)_2] \rightarrow Au_{52}(SR)_{32} + [Au_8(SR)_2] \rightarrow Au_{60}(SR)_{34} + [Au_8(SR)_2] \rightarrow Au_{68}(SR)_{36}$, are explored. The generic growth patterns underlying both sequences of nanoclusters can be viewed as sequential addition of four and three highly stable tetrahedral Au_4 units on the cores, respectively. In addition, density functional theory calculations show that these three newly predicted gold nanoclusters have very close formation energies with their adjacent structures, large highest occupied molecular orbital-lowest unoccupied molecular orbital (HOMO−LUMO) gaps, and all-positive harmonic vibration frequencies, indicating their high stabilities.

Introduction

The knowledge of structural evolution among thiolate-protected gold nanoclusters is beneficial for better understanding their structure–property relationship.[1–4] Thanks to the structural determination of $Au_{28}(TBBT)_{20}$ (TBBT = 4-*tert*-butyl-benzenethiolate), $Au_{36}(TBBT)_{24}$, $Au_{44}(TBBT)_{28}$, and $Au_{52}(TBBT)_{32}$, a "magic series" $Au_{8n+4}(TBBT)_{4n+8}$ (n = 3–6) with a uniform anisotropic growth pattern was identified as a typical case to investigate their size-dependent properties.[5,6] For example, the size-dependent quantum confinement nature understood by the empirical scaling law and classical "particle in a box" model and the redshift of the onset of the optical absorption spectra with the increment of cluster size can be observed in this "magic series". The femtonanosecond excited state dynamics of this "magic series" demonstrate that the relaxation of hot carriers and recombination of band-edge carriers will slow down as the size increases from $Au_{28}(TBBT)_{20}$ to $Au_{52}(TBBT)_{32}$. In addition, the evolution of the catalytic activity of the "magic series" $Au_{8n+4}(TBBT)_{4n+8}$ (n

= 3–5) can potentially be attributed to the periodic evolution in the inner cores.

Another important application for the understanding of structural evolution among thiolate-protected gold nanoclusters is to provide scientific evidence to rule-guided structure predictions of gold nanoclusters.[7–9] To date, ten groups of "magic series" of thiolate-protected gold nanoclusters have been identified, as shown in Table 1, resulting in a large number of structural predictions of gold clusters.[5,6,10–14] Particularly, among these predicted structures, two atomic structures of $Au_{44}(SR)_{28}$ and $Au_{36}(SR)_{24}$ were experimentally confirmed by X-ray crystallography.[15,16] For each "magic series" of thiolate-protected gold nanoclusters, their structural evolution can be viewed as the addition of a common motif or addition of several highly stable triangular Au_3 or tetrahedral Au_4 units on the cores. Taking the "magic series" $Au_{28+n}(SR)_{20-n}$ (n = 0–2) as an example, the structural evolution of $Au_{28}(SR)_{20}$, $Au_{29}(SR)_{19}$, and $Au_{30}(SR)_{18}$ can be viewed as sequential addition of a common motif $[Au(SR)_{-1}]$, namely $Au_{28}(SR)_{20} + [Au(SR)_{-1}] \rightarrow Au_{29}(SR)_{19} + [Au(SR)_{-1}] \rightarrow Au_{30}(SR)_{18}$, or sequential addition of one highly stable triangular Au_3 unit on the cores.

With the development of theoretical models, *i.e.*, the grand unified model (GUM) and ring model,[17,18] structural insights into the better understanding of thiolate-protected gold nanoclusters can be obtained, thereby providing theoretical tools to identify "magic series" of thiolate-protected gold nanoclusters with different common motifs. In the GUM, the gold cores of ligand-protected gold nanoclusters can be viewed as several

[a]*College of Energy Engineering, Xinjiang Institute of Engineering, Urumqi 830023, China. E-mail: wenliangli@vip.126.com*

[b]*Department of Physics, School of Physical Science and Technology, Ningbo University, Ningbo 315211, China. E-mail: xuwenwu@nbu.edu.cn*

† Electronic supplementary information (ESI) available: The cartesian coordinates of the three predicted thiolate-protected gold nanoclusters. See DOI: https://doi.org/10.1039/d3na00372h

‡ W. Han and G. Wang contributed equally to this work.

Table 1 Several groups of "magic series" of thiolate-protected gold nanoclusters as well as their common motifs and the number of units added on the core[a]

"Magic series" of gold nanoclusters	Common motif	Number of units added to the core	
		Triangular Au_3	Tetrahedral Au_4
$Au_{28+4n}(SR)_{20+2n}$ ($n = 0–6$)	$[Au_4(SR)_2]$	0	1
$Au_{28+n}(SR)_{20-n}$ ($n = 0–2$)	$[Au(SR)_{-1}]$	1	0
$Au_{44+24n}(SR)_{28+8n}$ ($n = 0–2$)	$[Au_{24}(SR)_8]$	0	8
$Au_{22+6n}(SR)_{18+2n}$ ($n = 0–3$)	$[Au_6(SR)_2]$	0	2
$Au_{40+9n}(SR)_{24+3n}$ ($n = 0–3$)	$[Au_9(SR)_3]$	0	3
$Au_{28+26n}(SR)_{20+14n}$ ($n = 0–4$)	$[Au_{26}(SR)_{14}]$	0	6
$Au_{36+36n}(SR)_{24+16n}$ ($n = 0–4$)	$[Au_{36}(SR)_{16}]$	0	10
$Au_{44+42n}(SR)_{28+18n}$ ($n = 0–4$)	$[Au_{42}(SR)_{18}]$	0	12
$Au_{52+52n}(SR)_{32+20n}$ ($n = 0–4$)	$[Au_{52}(SR)_{20}]$	0	16
$Au_{52+24n}(SR)_{32+10n}$ ($n = 0–4$)	$[Au_{24}(SR)_{10}]$	0	7
$Au_{44+12n}(SR)_{28+4n}$ ($n = 0–2$)*	$[Au_{12}(SR)_4]$	0	4
$Au_{44+8n}(SR)_{30+2n}$ ($n = 0–3$)*	$[Au_8(SR)_2]$	0	3

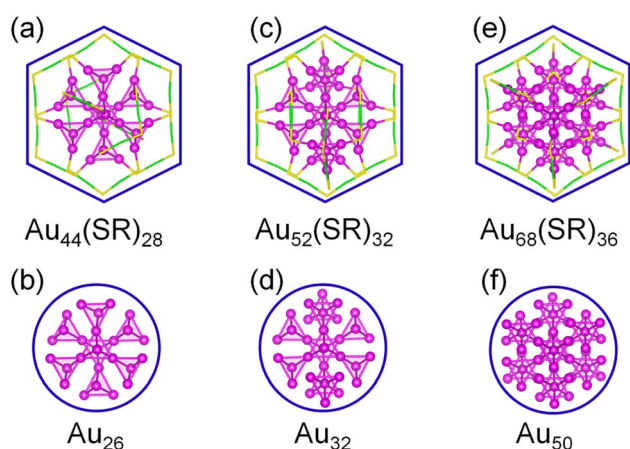[a] (*) denotes the newly identified "magic series" of thiolate-protected gold nanoclusters in this work.

Fig. 1 Structures and their gold cores of $Au_{44}(SR)_{28}$ (a and b), $Au_{52}(SR)_{32}$ (c and d), and $Au_{68}(SR)_{36}$ (e and f) nanoclusters.
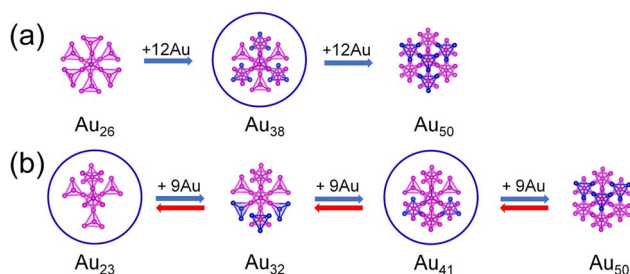

Fig. 2 The construction of new Au_{38}, Au_{23}, and Au_{41} cores (a and b). Au: magenta and blue, respectively. The blue atoms are the added gold atoms.

triangular Au_3(2e) or tetrahedral Au_4(2e) elementary blocks packing or fusing together.[19] Meanwhile in the ring model, the interfacial interactions between SR $[Au(SR)]_x$ ($x = 0, 1, 2, 3,…$) protection motifs and gold cores in thiolate-protected gold nanoclusters can be understood by several $[Au_m(SR)_n]$ ($m = 4–8$,

10, 12, and $0 \leq n \leq m$) rings. Based on the GUM and ring model, some thiolate-protected gold nanoclusters, such as $Au_{15}(SR)_{13}$, $Au_{22}(SR)_{16}$, and $Au_{30}(SR)_{20}$, were predicted to have high stability.[20–22] In this paper, based on the GUM and ring model, two new groups of "magic series" of thiolate-protected gold nanoclusters ($Au_{44+8n}(SR)_{30+2n}$ ($n = 0–3$) and $Au_{44+16n}(SR)_{28+4n}$ ($n = 0–2$)) were identified via structural predictions of three medium-sized nanoclusters ($Au_{44}(SR)_{30}$, $Au_{56}(SR)_{32}$, and $Au_{60}(SR)_{34}$).

Results and discussion

We focused on three thiolate-protected gold nanoclusters $Au_{44}(SR)_{28}$, $Au_{52}(SR)_{32}$, and $Au_{68}(SR)_{36}$, and found an interesting phenomenon: a top view of these structures reveals that they are hexagonal, while their gold cores are round (Fig. 1),[23–25] suggesting that $Au_{44}(SR)_{28}$, $Au_{52}(SR)_{32}$, and $Au_{68}(SR)_{36}$ have very similar morphology. In addition, these thiolate-protected gold nanoclusters follow the grand unified model (GUM) and their gold cores can be regarded as several tetrahedral Au_4 elementary blocks following the duet rule.[17,18] This interesting phenomenon led us to ponder the question: Are there other new intermediate structures with similar morphology between these thiolate-protected gold nanoclusters?

In Fig. 2, the Au_{26} core of $Au_{44}(SR)_{28}$ is formed by the face-to-face combination of two Au_{13} units, which can be regarded as four tetrahedral Au_4 fusing together by sharing three Au atoms. The Au_{50} core of $Au_{68}(SR)_{36}$ nanoclusters is composed of two Au_{25} units, which can be decomposed into eight tetrahedral Au_4 fusing together by sharing seven Au atoms. Thus, the Au_{26} core fused with four tetrahedral Au_4 (blue atoms in Fig. 2a) or the Au_{50} core removed four tetrahedral Au_4 (blue atoms in Fig. 2a) will form a new Au_{38} core. In the same way, a new Au_{41} and Au_{23} core can be formed by removing three tetrahedral Au_4 (blue atoms in Fig. 2b) from the Au_{50} core of $Au_{68}(SR)_{36}$ nanoclusters or the Au_{32} core of $Au_{52}(SR)_{32}$ nanoclusters. It can be seen from the top view in Fig. 2 that these new cores are all round.
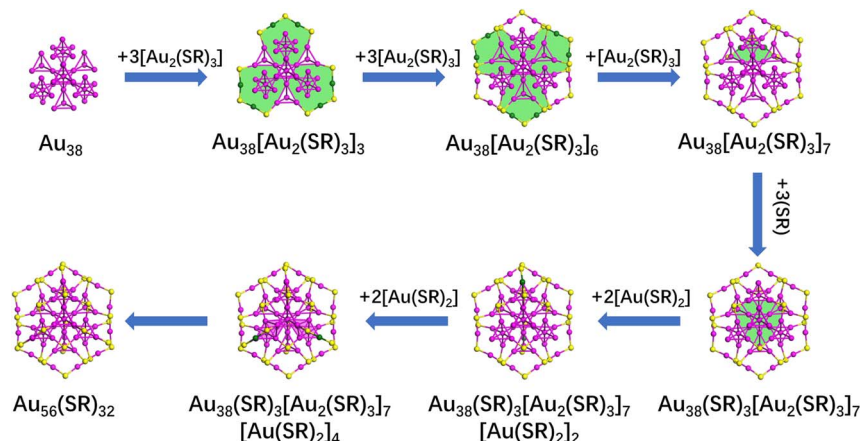
Fig. 3 The structural prediction of a new structure $Au_{56}(SR)_{32}$ based on the ring model and GUM. The rings are filled with green color, and Au (111) facets are filled with wine color. Au: wine and dark green; S: yellow. The R groups are omitted for clarity.

Employing the newly constructed Au_{38}, Au_{23}, and Au_{41} cores, new structures of thiolate-protected gold nanoclusters can be predicted by the GUM and ring model. In Fig. 3, the process for the Au_{38} core involves several steps. Initially, three $[Au_2(SR)_3]$ protection motifs are added around the Au_{38} core, resulting in the formation of three $[Au_6(SR)_3]$ rings and an $Au_{38}[Au_2(SR)_3]_3$ structure. Subsequently, three $[Au_2(SR)_3]$ protection motifs are further added around the structure $Au_{38}[Au_2(SR)_3]_3$, forming three $[Au_6(SR)_3]$ rings and an $Au_{38}[Au_2(SR)_3]_6$ structure. In the third step, $[Au_2(SR)_3]$ protection motifs are incorporated behind the structure $Au_{38}[Au_2(SR)_3]_6$, resulting in the formation of a single $[Au_6(SR)_3]$ ring and $Au_{38}[Au_2(SR)_3]_7$ structure. Then, in the fourth step, three $[SR]$ molecules are added to the middle of the structure $Au_{38}[Au_2(SR)_3]_7$, forming another $[Au_6(SR)_3]$ ring and $Au_{38}(SR)_3[Au_2(SR)_3]_7$ structure. Finally, the structure $Au_{38}(SR)_3[Au_2(SR)_3]_7$ undergoes the addition of four $[Au(SR)_2]$ protection motifs, leading to the prediction of a new structure, $Au_{56}(SR)_{32}$. Since the structure is the intermediate structure between $Au_{44}(SR)_{28}$ and $Au_{68}(SR)_{36}$, a new evolutionary path $Au_{44+8n}(SR)_{30+2n}$ ($n = 0–3$) was identified.

In Fig. 4, we illustrate the structure prediction of another gold nanocluster starting from an Au_{41} core. Initially, six $[Au_2(SR)_3]$ protective motifs were introduced, resulting in the formation of six $[Au_6(SR)_3]$ rings and an $Au_{41}[Au_2(SR)_3]_6$ structure. Subsequently, three $[SR]$ ligands were added, leading to the creation of a single $[Au_6(SR)_3]$ ring and $Au_{41}[Au_2(SR)_3]_6[SR]_3$ structure. Next, two $[Au(SR)_2]$ ligands were further added to $Au_{41}[Au_2(SR)_3]_6[SR]_3$ to form two $[Au_6(SR)_2]$ rings and an $Au_{41}[SR]_3[Au_2(SR)_3]_6[Au(SR)_2]_2$ structure. Finally, one $[Au_2(SR)_3]$ and three $[Au(SR)_2]$ ligands were bonded to the $Au_{41}[SR]_3[Au_2(SR)_3]_6[Au(SR)_2]_2$ structure to achieve the full structure prediction of $Au_{60}(SR)_{34}$. Since the structure is the intermediate structure between $Au_{52}(SR)_{32}$ and $Au_{68}(SR)_{36}$, a new evolutionary path $Au_{44+8n}(SR)_{30+2n}$ ($n = 1–3$) was identified. In addition, the structure prediction of $Au_{44}(SR)_{30}$ nanoclusters starting from the Au_{23} core is presented in Fig. 5 following the same way as the structure prediction of $Au_{56}(SR)_{32}$ and $Au_{60}(SR)_{34}$. Interestingly, the structure of $Au_{44}(SR)_{30}$ nanoclusters can be brought into the evolutionary path of $Au_{44+8n}(SR)_{30+2n}$ ($n = 0–3$).

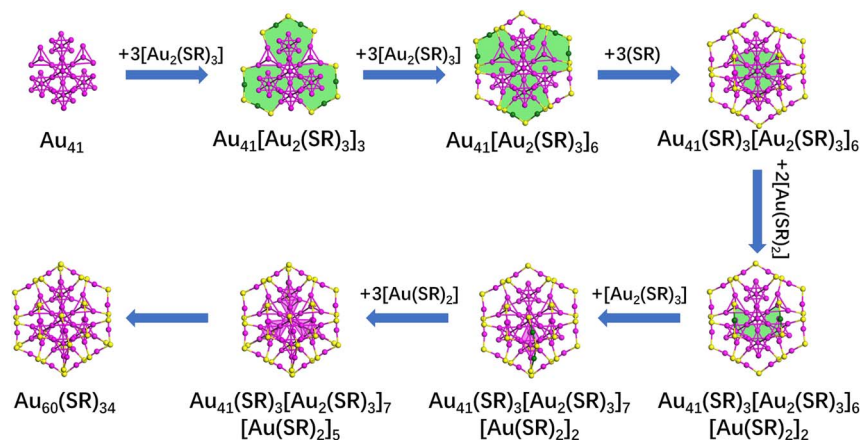**Fig. 4** The structural prediction of a new $Au_{60}(SR)_{34}$ isomer based on the ring model and GUM. The rings are filled with green color and Au (111) facets are filled with wine color. Au: wine and dark green; S: yellow. The R groups are omitted for clarity.
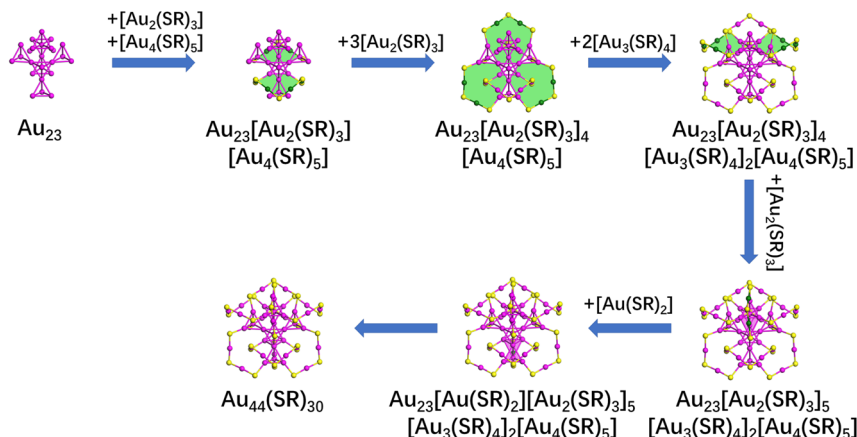
Fig. 5 The structural prediction of a new structure $Au_{44}(SR)_{30}$ based on the ring model. The rings are filled with green color and Au (111) facets are filled with wine color. Au: wine and dark green; S: yellow. The R groups are omitted for clarity.

Table 2 The calculated HOMO–LUMO gaps and the lowest vibrational and frequencies of two magic series $Au_{44+8n}(SR)_{30+2n}$ ($n = 0-3$) and $Au_{44+12n}(SR)_{28+4n}$ ($n = 0-2$)

Structures	HOMO–LUMO gaps/eV	Lowest vibrational frequency/cm^{-1}
$Au_{44}(SR)_{28}$	1.660	11.120
$Au_{44}(SR)_{30}$	1.714	7.491
$Au_{52}(SR)_{32}$	1.470	6.737
$Au_{56}(SR)_{32}$	1.361	10.680
$Au_{60}(SR)_{34}$	1.333	8.162
$Au_{68}(SR)_{36}$	1.170	—

Employing Gaussian 09 software,[26] density general function theory (DFT) calculations for $Au_{44+8n}(SR)_{30+2n}$ ($n = 0-3$) and $Au_{44+12n}(SR)_{28+4n}$ ($n = 0-2$) were performed to obtain the electronic properties of $Au_{44}(SR)_{30}$, $Au_{56}(SR)_{32}$, and $Au_{60}(SR)_{34}$ structures. In all calculations, the Perdew–Burke–Ernzerhof (PBE) and the all-electron basis set 6-31G* for H and S, and effective-core basis set LANL2DZ pseudopotential groups for Au were adopted.[27,28] In addition, the R groups were simplified with H atoms in order to save computational costs. In Table 2, the computed harmonic vibrational frequencies of three new structures as well as other two reported structures are all positive, which indicates that these structures are located at the local minima of potential energy surfaces. The highest occupied molecular orbital-lowest unoccupied molecular orbital (HOMO–LUMO) gaps of the predicted nanoclusters are 1.71, 1.36, and 1.33 eV, respectively. The large HOMO–LUMO gaps and all-positive harmonic vibrational frequencies suggest that the predicted structures have high chemical stability. Furthermore, the formation energy $E = E_{(n-1)} + E_{(n+1)} - E_{(n)}$ of these newly predicted structures in two magic series $Au_{44+8n}(SR)_{30+2n}$ ($n = 0-3$) and $Au_{44+12n}(SR)_{28+4n}$ ($n = 0-2$) was calculated. The results show that the formation energies of $Au_{44}(SR)_{30}$, $Au_{56}(SR)_{32}$, and $Au_{60}(SR)_{34}$ structures are 0.50, 0.26, and 0.04 eV, respectively, suggesting their very close stability to their adjacent nanoclusters.

The superatom network model with natural density zoning (AdNDP) analysis was always employed to describe thiolate-protected gold nanoclusters.[29] Taking the Au_{23}^{9+} core of

$Au_{44}(SR)_{30}$ in Fig. 6 as an example, the 14 valence electrons of $Au_{44}(SR)_{30}$ can be viewed to be equally distributed on seven Au_4 units. Therefore, the Au_{23}^{9+} core of $Au_{44}(SR)_{30}$ can be regarded as a network of seven 4c–2e (4c and 2e represent 4 centers and 2 electrons, respectively) units. A similar behaviour can also be seen in the $Au_{(23+9n)}^{(9+3n)+}$ core of $Au_{44+8n}(SR)_{30+2n}$ ($n = 0-3$) and the $Au_{(26+12n)}^{(10+4n)+}$ core of $Au_{44+12n}(SR)_{28+4n}$ ($n = 0-2$) nanoclusters (Fig. 6).

In Fig. 7 and 8, the optical absorption spectra and corresponding Kohn–Sham (KS) orbital energy levels of six nanoclusters computed by the time-dependent DFT (TD-DFT) method at the PBE/LANL2DZ level are shown. In addition, 300 singlet states were included in all TD-DFT calculations. Taking $Au_{56}(SR)_{32}$ in Fig. 7 as an example, $Au_{56}(SR)_{32}$ shows two broad peaks at 672 and 875 nm. The absorption peak at 875 nm mainly stems from the HOMO to LUMO, LUMO+1, and LUMO+2, and the absorption peak at 672 nm mainly stems
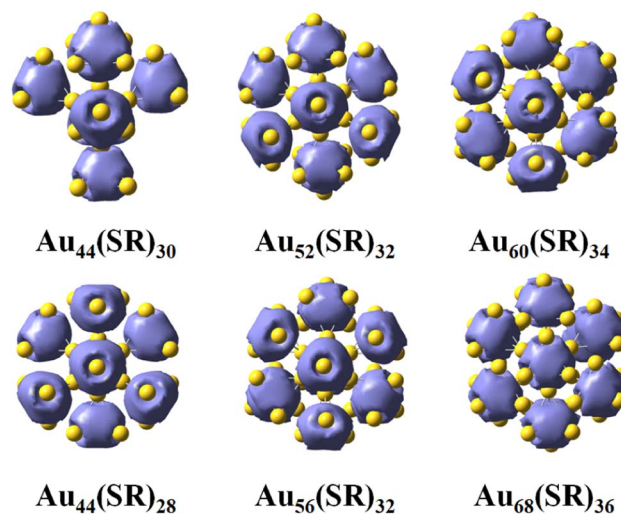

Fig. 6 Visualization of the valence electron distributions in the $Au_{(23+9n)}^{(9+3n)+}$ core of $Au_{44+8n}(SR)_{30+2n}$ ($n = 0-3$) and the $Au_{(26+12n)}^{(10+4n)+}$ core of $Au_{44+12n}(SR)_{28+4n}$ ($n = 0-2$) nanoclusters. Au atoms are presented in yellow.
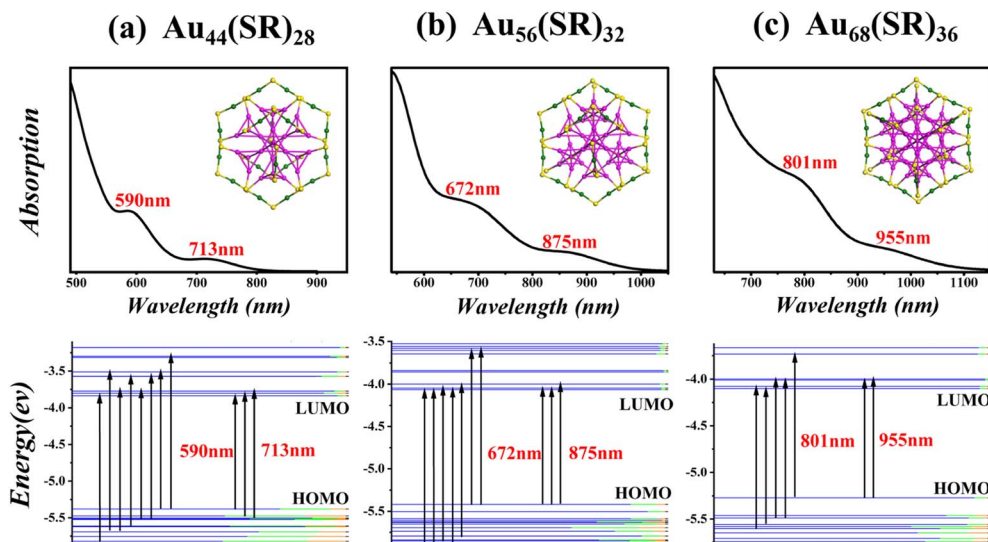
Fig. 7 The calculated optical absorption spectra and energy leap spectra of structures in the magic series $Au_{44+12n}(SR)_{28+4n}$ ($n = 0-2$). The lines in blue, green, red, and black represent the 6sp of Au, 5d of Au, 3p of S, and others, respectively.
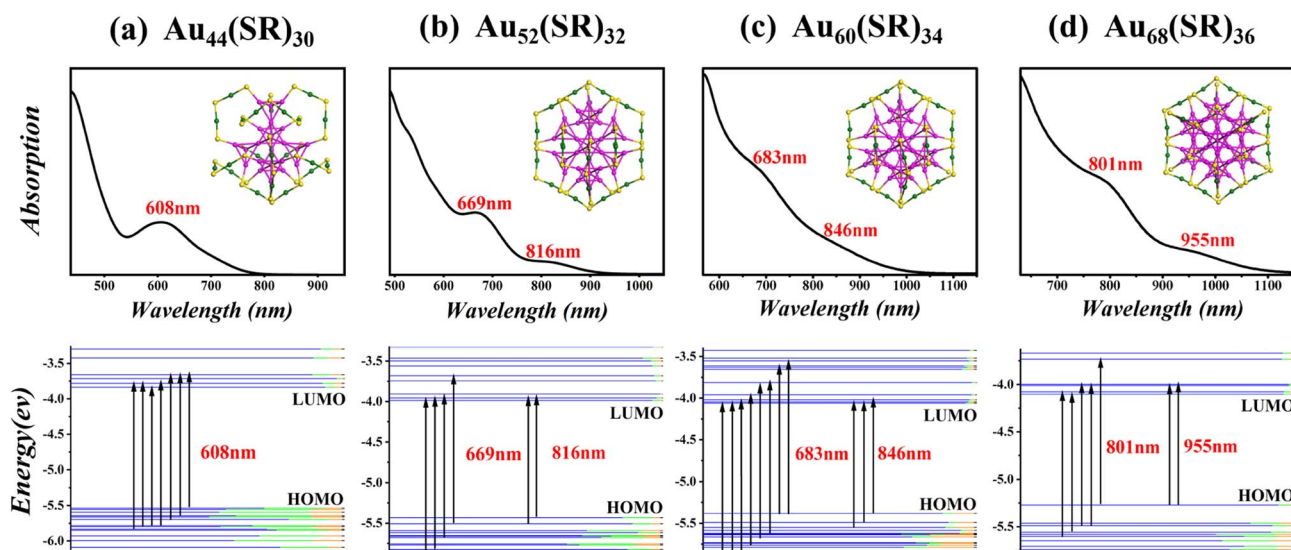

Fig. 8 The calculated optical absorption spectra and energy leap spectra of structures in the magic series $Au_{44+8n}(SR)_{30+2n}$ ($n = 0-3$). The lines in blue, green, red, and black represent the 6sp of Au, 5d of Au, 3p of S, and others, respectively.

from HOMO to LUMO+7 and LUMO+8, HOMO−7 and HOMO−8 to LUMO+2, HOMO−10 to LUMO+1, and HOMO−9 and HOMO−10 to LUMO. In addition, the absorption peaks of all the nanoclusters in Fig. 7 and 8 mainly involve the Au(sp) → Au(sp) transitions, which may be attributed to their similar morphology.

Conclusions

In summary, we have predicted the theoretical structures of three medium-sized nanoclusters $Au_{44}(SR)_{30}$, $Au_{56}(SR)_{32}$, and $Au_{60}(SR)_{34}$ based on the GUM and ring model, resulting in two new magic series $Au_{44+8n}(SR)_{30+2n}$ ($n = 0-3$) and $Au_{44+16n}(SR)_{28+4n}$ ($n = 0-2$). DFT calculations show that the predicted structures have high

chemical stability and are likely to be synthesized in the laboratory. Our work further proves the high reliability and practicality of the GUM and ring model in designing the structures of thiolate-protected gold nanoclusters.

Conflicts of interest

The authors declare no conflicts of interest.

Acknowledgements

References

1 D. Yang and Y. Zhu, *Chin. J. Catal.*, 2021, **42**, 245–250.

2 Y. Pei, P. Wang, Z. Ma and L. Xiong, *Acc. Chem. Res.*, 2019, **52**, 23–33.

3 W. W. Xu, Y. Li, Y. Gao and X. C. Zeng, *Nanoscale*, 2016, **8**, 7396–7401.

4 S. Chen, L. Xiong, S. Wang, Z. Ma, S. Jin, H. Sheng, Y. Pei and M. Zhu, *J. Am. Chem. Soc.*, 2016, **138**, 10754–10757.

5 C. Zeng, Y. Chen, K. Iida, K. Nobusada, K. Kirschbaum, K. J. Lambright and R. Jin, *J. Am. Chem. Soc.*, 2016, **138**, 3950–3953.

6 M. Zhou, C. Zeng, M. Y. Sfeir, M. Cotlet, K. Iida, K. Nobusada and R. Jin, *J. Chem. Phys.*, 2017, **8**, 4023–4030.

7 W. W. Xu, X. Duan and X. C. Zeng, *J. Phys. Chem. Lett.*, 2020, **11**, 536–540.

8 X. Sun, P. Wang, L. Xiong and Y. Pei, *Chem. Phys. Lett.*, 2018, **704**, 68–75.

9 P. Liu, W. Han, M. Zheng and W. W. Xu, *Nanoscale*, 2020, **12**, 20677–20683.

10 M. Zhou, R. Jin, M. Y. Sfeir, Y. Chen, Y. Song and R. Jin, *Proc. Natl. Acad. Sci. U. S. A.*, 2017, **114**, E4697–E4705.

11 L. Yang, P. Wang, Z. Yang and Y. Pei, *Nanoscale*, 2020, **12**, 5554–5566.

12 Y. Sun, E. Wang, Y. Ren, K. Xiao, X. Liu, D. Yang, Y. Gao, W. Ding and Y. Zhu, *Adv. Funct. Mater.*, 2019, **29**, 1904242.

13 Q. Li, M. Zhou, W. Y. So, J. Huang, M. Li, D. R. Kauffman, M. Cotlet, T. Higaki, L. A. Peteanu, Z. Shao and R. Jin, *J. Am. Chem. Soc.*, 2019, **141**, 5314–5325.

14 X. Du, J. Chai, S. Yang, Y. Li, T. Higaki, S. Li and R. Jin, *Nanoscale*, 2019, **11**, 19158–19165.

15 X. Liu, W. W. Xu, X. Huang, E. Wang, X. Cai, Y. Zhao, J. Li, M. Xiao, C. Zhang, Y. Gao, W. Ding and Y. Zhu, *Nat. Commun.*, 2020, **11**, 3349.

16 C. Zeng, Y. Chen, G. Li and R. Jin, *Chem. Commun.*, 2014, **50**, 55–57.

17 W. Han, P. Liu, M. Zheng, X. C. Zeng and W. W. Xu, *J. Phys. Chem. Lett.*, 2021, **12**, 3006–3013.

18 W. W. Xu, B. Zhu, X. C. Zeng and Y. Gao, *Nat. Commun.*, 2016, **7**, 13574.

19 W. W. Xu, X. C. Zeng and Y. Gao, *Acc. Chem. Res.*, 2018, **51**, 2739–2747.

20 Y. Liu, W. Han, Z. Hong, W. W. Xu and E. Wang, *J. Phys. Chem. Lett.*, 2022, **13**, 5387–5393.

21 W. Han, E. Wang and W. W. Xu, *Phys. Chem. Chem. Phys.*, 2022, **24**, 15920–15924.

22 P. Liu, W. Han, M. Zheng, W. Li, J. Ren, A. Tlahuice-Flores and W. W. Xu, *J. Phys. Chem. A*, 2021, **125**, 5933–5938.

23 Y. Pei, S. Lin, J. Su and C. Liu, *J. Am. Chem. Soc.*, 2013, **135**, 19060–19063.

24 P. Wang, X. Sun, X. Liu, L. Xiong, Z. Ma and Y. Pei, *J. Phys. Chem. Lett.*, 2017, **8**, 1248–1252.

25 S. Zhuang, L. Liao, M.-B. Li, C. Yao, Y. Zhao, H. Dong, J. Li, H. Deng, L. Li and Z. Wu, *Nanoscale*, 2017, **9**, 14809–14813.

26 G. W. T. M. J. Frisch, H. B. Schlegel, G. E. Scuseria, M. A. Robb, J. R. Cheeseman, G. Scalmani, V. Barone, G. A. Petersson, H. Nakatsuji, X. Li, M. Caricato, A. Marenich, J. Bloino, B. G. Janesko, R. Gomperts, B. Mennucci, H. P. Hratchian, J. V. Ortiz, A. F. Izmaylov, J. L. Sonnenberg, D. Williams-Young, F. Ding, F. Lipparini, F. Egidi, J. Goings, B. Peng, A. Petrone, T. Henderson, D. Ranasinghe, V. G. Zakrzewski, J. Gao, N. Rega, G. Zheng, W. Liang, M. Hada, M. Ehara, K. Toyota, R. Fukuda, J. Hasegawa, M. Ishida, T. Nakajima, Y. Honda, O. Kitao, H. Nakai, T. Vreven, K. Throssell, J. A. Montgomery Jr, J. E. Peralta, F. Ogliaro, M. Bearpark, J. J. Heyd, E. Brothers, K. N. Kudin, V. N. Staroverov, T. Keith, R. Kobayashi, J. Normand, K. Raghavachari, A. Rendell, J. C. Burant, S. S. Iyengar, J. Tomasi, M. Cossi, J. M. Millam, M. Klene, C. Adamo, R. Cammi, J. W. Ochterski, R. L. Martin, K. Morokuma, O. Farkas, J. B. Foresman and D. J. Fox, *Gaussian 09, revision D*, Gaussian, Inc., Wallingford, CT, 2010.

27 M. Caricato, B. Mennucci, G. Scalmani, G. W. Trucks and M. J. Frisch, *J. Chem. Phys.*, 2010, **132**, 084102.

28 J. P. Perdew, K. Burke and M. Ernzerhof, *Phys. Rev. Lett.*, 1996, **77**, 3865–3868.

29 L. Cheng, Y. Yuan, X. Zhang and J. Yang, *Angew. Chem., Int. Ed. Engl.*, 2013, **52**, 9035–9039.